Simulation of Slip Effect with 4:1 Contraction Flow for Oldroyd-B Fluid

Thongjub N.

Department of Mathematics and Computer Science, Faculty of Science, Chulalongkorn University, Bangkok, Thailand

Puangkird B.

Department of Mechanical Engineering, Faculty of Engineering, KMITL, Bangkok, Thailand

Ngamaramvaranggul V.

Department of Mathematics and Computer Science, Faculty of Science, Chulalongkorn University, Bangkok, Thailand
E-mail address: Vimolrat.N@chula.ac.th

Abstract

The slip effect of 4:1 contraction problem for Oldroyd-B fluid is determined to reduce the stress values and vortex size after the Navier-Stokes equation was solved with planar coordinate system. The numerical solutions of no slip and slip condition are calculated by semi-implicit Taylor-Galerkin pressure-correction finite element method. The slip velocity at channel wall is adjusted after each time step. The velocity gradient recovery and streamline-Upwind/Petrov-Galerkin schemes are employed to keep the unique values and stabilize the converged solutions, respectively. The flow patterns are shown in streamline contour and vortex.

Keywords: slip effect, 4:1 contraction, Oldroyd-B fluid

1 Introduction

This research is concentrated upon the application of the slip effect for Oldroyd-B constitutive model in the area of 4:1 contraction flows to adopt a semi-implicit Taylor-Galerkin pressure-correction finite element method (STGFEM) as a tool for solving a problem for this flow. The influence of shear stress in sharp corner 4:1 contraction domains is analyzed and corrected by adding the slip function on the boundary of channel wall.

The 4:1 contraction flow is a well know problem to discover kinematic behavior of viscoelastic flows whilst flow path has sudden change in the kind of this geometry especially for two-dimensional system. There are strong elongation and violent shear stress at contraction position. The experimental work, in 1972 Boger and Ramamurhy [1] have observed the rheological properties in upstream of a 2 to 1 contraction. After that Boger and Denn [2] have measured the pressure drop and normal stresses for low Reynolds numbers in capillary and slit method. Walters and Rawlinson [3] have illustrated the results

of planar contraction flows for Boger fluid. Boger [4] has presented the experiment and numerical results of circular contraction for both Newtonian and Non-Newtonian fluids in 1987.

Instead of solving analytic solution of viscoelastic problem through which it is extremely hard to find the non-linear partial differential equations in the mathematical model of the conservation of mass and momentum equations (including constitutive equation); one can utilize the numerical techniques which can efficiently eliminate inconvenient problems. In this style, there are various useful methods such as finite difference method (FDM), finite element method (FEM), and finite volume method (FVM) to calculate the approximate solution. In 1999, Phillips and Williams [5] applied a semi-Lagrangian FVM to solve a 4:1 planar contraction of Oldroyd-B fluid for inert and inertial flows. Shortly after, they [4] have typically using different data of the same problem by expanding a new axisymmetric flow but this time the grids have been fixed in

Eulerian methods. Aboubacar et al. [7,8] have shown the technique of a cell-vertex hybrid finite volume/element method, which is appropriate to compute highly elastic solutions for Oldroyd-B and Phan-Thien/Tanner (PTT) fluids with rounded and sharp corner contraction figures. Alves et al. [9] have selected the FVM to calculate creeping PTT flow past planar abrupt contractions and make clear that Deborah numbers and contraction ratios are dependent on flow characteristics.

A lot of problems that have been solved by FEM are as following papers. In 2001, Ngamaramvaranggul and Webster [10] adopted FEM for stick-slip problem of Oldroyd-B fluid and they added free surface method after final solution of stick-slip flow to adjust the streamline path for swelling so the updated flow is Die-swell problem and they found that swelling ratio is varied as a function of relaxation time. Shortly After, they [11] calculated Phan-Thien/Tanner fluid with the complex geometry of pressure-tooling wire-coating die via employment of the same standard FEM and streamline-upwind Petrov/Galerkin (SUPG). In 2007, Belblidia et al. [12] have applied alternate subcell to interpolate cooperative stress via FV/FE method for calculation of cavity and contraction flows with Oldroyd fluid. After that, Puangkird et al. [13] have investigated the sufficient various schemes to consider constitutive models and rheological properties in cross-slot devices though FV/FE pressure correction method.

Since the difference between experiment and numerical solution for fluid flows through hard wall is significant so the study of fluid particle speed on solid surface is determine to slip instead of stick. A numerical study of Newtonian and viscoelastic flow on slip effect for free surface has been cited by Silliman and Scriven [14]. This result got along well with the next experiment of Ramamurthy [15] who has focused on surface melt fracture of HDPE and LLDPE that is the outcome from slip in die land. Previously, both slip cases had been supported strongly with analysis solution of Jiang et al. [16] by setting slip velocity for capillary tubes as a function of wall shear stress as well as Phan-Thien [17] who manifested the same concept of slip velocity, which is a function of wall shear stress. However, slip velocity comes still into notice if the critical shear stress is less than wall shear stress. In 2000, Ngamaramvaranggul and Webster [18] have driven the slip effect scheme to consider the free surface in tube-tooling and pressure-tooling die problems.

In this research, the slip effect scheme has been considered in the problem of 4:1 contraction for Newtonian and Oldroyd-B fluids under the two-dimensional planar isothermal incompressible flow and formed the mathematical model of Navier-Stokes equations by means of STGFEM. Besides, the velocity gradient recovery and the streamline-upwind Petrov/Galerkin (SUPG) techniques have been chosen to stabilize the converged solutions. Finally, the solutions have been considered with and without the slip condition by means of Phan-Thien slip rule, which is a relation between shear stress and velocity at wall. The stress value and vortex size of slip condition were compared with Johnson and Segalman model [19].

2 Governing equations

The conservation of mass and momentum for incompressible fluid of viscoelastic flow under non gravity is preserved in Navier-Stokes equations with measure unit in different quantity from other literatures so the normalization of unit has been proposed to present in non-dimensional system, which is a standard for benchmark. The derivative equations of continuity equation (1) and kinematic equation (2) have been transformed to dimensionless system as.

$$\nabla \cdot \boldsymbol{U} = 0 \qquad (1)$$

$$\text{Re}\boldsymbol{U}_t = \nabla \cdot \boldsymbol{T} - \text{Re}\,\boldsymbol{U} \cdot \nabla \boldsymbol{U} - \nabla P \qquad (2)$$

where ∇ is the differential operator, $\boldsymbol{U}$ is velocity vector, $\boldsymbol{U}_t$ is time derivative of $\boldsymbol{U}$, P is pressure, and the extra-stress tensor $\boldsymbol{T} = \boldsymbol{\tau} + 2\mu_2\tilde{\boldsymbol{D}}$, $\boldsymbol{\tau}$ is the polymeric component of the extra-stress tensor, $\tilde{\boldsymbol{D}} = \left[\nabla\boldsymbol{U} + \left(\nabla\boldsymbol{U}\right)^T\right]\big/2$ the rate of deformation tensor, and Reynolds number $\text{Re} = \rho V L\big/\mu_0$, Here, ρ is the fluid density, V is the characteristic velocity, L is the characteristic length in terms of channel width and μ_0 is the zero-shear viscosity which $\mu_0 = \mu_1 + \mu_2$ where μ_1 is the polymeric viscosity and μ_2 is the solvent viscosity. The non-dimensional constants are $\text{Re} = 0$, $\mu_1 / \mu_0 = 0.88$ and $\mu_2 / \mu_0 = 0.12$.

The non-dimensional constitutive equation of a viscoelastic fluid for Oldroyd-B model is

$$We\boldsymbol{\tau}_t = 2\mu_1 \boldsymbol{D} - \boldsymbol{\tau} + We\left[\boldsymbol{\tau}\cdot\nabla U + \left(\nabla U\right)^T\cdot\boldsymbol{\tau} - U\cdot\nabla\boldsymbol{\tau}\right] \quad (3)$$

where We is the non-dimensional Weissenberg number, $We = \lambda_1 V / L$, λ_1 is the relaxation time and $(\ )^T$ is the transpose operator .

For convenience to calculate the shear stress (τ_{xy}) of Oldroyd-B fluid, Johnson and Segalman [19] have applied shear stress as a function of shear viscosity (η) and shear rate ($\dot{\gamma}$) on the basis of the kinematic theory of macro-molecules.

$$\tau_{xy} = \frac{\eta_1 \dot{\gamma}}{1 + a(2-a)(\lambda_1 \dot{\gamma})^2} + \eta_2 \dot{\gamma} \quad (4)$$

where η_1 and η_2 are viscosity coefficients and a is a scalar parameter between $(0, 2)$.

3 Numerical Scheme

Normally, the non-linear differential Equations (2) and (3) are hardly to solve by analysis method and many cases cannot be calculated directly so some numerical technique are proposed to operate especially FEM, which is a tool for this problem. A few complex procedures are conducted to compute the convection terms of Navier-Stokes equation (2) and the constitutive equation of Oldroyd-B model (3) by means of below scheme STGFEM that is a method to split both the equations into half time step. Since the continuous equations (2) and (3) are converted to discretization equations and formulated to system of linear equation, the proximate solution is calculated by Jacobi iterative method and Cholesky decomposition scheme.

3.1 *Semi-implicit Taylor-Galerkin pressure-correction finite element method*

To solve convection equations conveniently, the perfect union of factional time steps and FEM is applied to split non-dimensional equations (2) and (3) for three stages per time step as below classification. This cumulated scheme is known as semi-implicit Taylor-Galerkin pressure-correction finite element method (STGFEM).

Step 1a :

$$\left(2\frac{\text{Re}}{\Delta t}\right)\left(U^{n+1/2} - U^n\right) = -\left(\text{Re}\,U\cdot\nabla U - \nabla P\right)^n$$

$$+\left[\nabla\cdot\left(\boldsymbol{\tau} + 2\mu_2\boldsymbol{D}\right)^n\right] + \nabla\cdot\mu_2\left(\boldsymbol{D}^{n+1/2} - \boldsymbol{D}^n\right) \quad (5)$$

$$\left(2\frac{We}{\Delta t}\right)\left(\boldsymbol{\tau}^{n+1/2} - \boldsymbol{\tau}^n\right) = \left(2\mu_1\boldsymbol{D} - \boldsymbol{\tau}\right)^n$$

$$+ We\left[\boldsymbol{\tau}\cdot\nabla U + \left(\nabla U\right)^T\cdot\boldsymbol{\tau} - U\cdot\nabla\boldsymbol{\tau}\right]^n \quad (6)$$

Step 1b :

$$\left(\frac{\text{Re}}{\Delta t}\right)\left(U^* - U^n\right) = \left(\nabla\cdot\boldsymbol{\tau} - \text{Re}\,U\cdot\nabla U\right)^{n+1/2}$$

$$+ \nabla\cdot\mu_2\left(\boldsymbol{D}^* - \boldsymbol{D}^n\right) + \left[\nabla\cdot\left(2\mu_2\boldsymbol{D}\right) - \nabla P\right]^n \quad (7)$$

$$\left(\frac{We}{\Delta t}\right)\left(\boldsymbol{\tau}^{n+1} - \boldsymbol{\tau}^n\right) = \left(2\mu_1\boldsymbol{D} - \boldsymbol{\tau}\right)^{n+1/2}$$

$$+ We\left(\boldsymbol{\tau}\cdot\nabla U + \left(\nabla U\right)^T\cdot\boldsymbol{\tau} - U\cdot\nabla\boldsymbol{\tau}\right)^{n+1/2} \quad (8)$$

Step 2 :

$$\nabla^2\left(P^{n+1} - P^n\right) = \left(\frac{2\text{Re}}{\Delta t}\right)\nabla U^* \quad (9)$$

Step 3 :

$$\left(2\frac{\text{Re}}{\Delta t}\right)\left(U^{n+1} - U^*\right) = -\left(P^{n+1} - P^n\right) \quad (10)$$

The partial differential equations (5)-(10) are discretised with FDM and FEM. The left for time derivative term is expanded by Taylor series and the right for spatial component is adopt weight residual of Galerkin finite element method so the equations of stages (1)-(3) are converted to the system of linear equations. The geometrical region of flow is designed to a network of small triangular elements in order to get the precise solution before approximate solution is solved with Jacobi iterative method for steps 1 and 3, and Cholesky decomposition for step 2.

3.2 *Phan-Thien slip rule*

To reduce shear stress at sharp corner point, Phan-Thien [17] have introduced the slip velocity at solid wall by setting the particle speed as a function of wall shear stress to make solution more precisely and close to the experimental outcome. The slip velocity will be calculated if some values of wall shear stress are greater than a constant critical shear value. This desired function is of the form

$$V_{slip} = V_{mean}\left[1-\exp\left(-\alpha\frac{\tau_w}{\tau_{crit}}\right)\right] \quad (11)$$

where V_{slip} is the slip velocity, V_{mean} is the mean velocity flowrate for no slip case, α is the constant slip coefficient, τ_w is the wall shear stress and τ_{crit} is the critical shear stress.

4 Problem Specification

There is a benchmark of slip and no slip cases in the same geometrical domain for 4:1 contraction flow that is normally used in industrial processes so the major body is picked in the model of sharp corner shape. The geometries of planar 4:1 contraction for the downstream half channel width *L* at entry and exit sections of 27.5*L* and 49*L* respectively are presented in Figure 1.
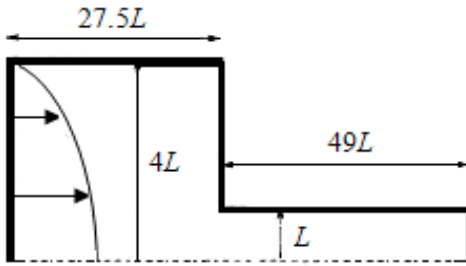
Figure 1: Schematic of 4:1 shape contraction flow.

The upstream inlet length is imposed to Poiseuille flow and fluid passes in channel, which is long enough to complete developing flow so the downstream exit length is still retaining parabolic flow pattern. At the channel wall, the slip condition is applied to gain intensive result close on real problem.

At inlet fully developed flow, the velocity in *x* direction, which is denoted *u* is varied with distance *y* that is null at the symmetrical line while normal and shear stresses are function of partial derivative of *u* hence the initial conditions for entrance boundary are imposed by equation (12).

$$u(y) = \frac{3}{128}(16 - y^2)\,, \; v = 0 \quad (12)$$

$$\tau_{xx} = 2We\,\mu_1\left(\frac{\partial u}{\partial y}\right)^2, \; \tau_{yy} = 0, \text{ and } \tau_{xy} = \mu_1\frac{\partial u}{\partial y}$$

Table 1: Mesh characteristics

Meshes	Element	Nodes	Degree of freedom	h_{min}
mesh1	980	2105	11088	0.025
mesh2	1140	2427	12779	0.023
mesh3	2987	6220	32717	0.006
mesh4	5140	10575	55593	0.004

To inspect the severe stress at impact wall, the sharp corner contraction mesh1-mesh4 are considered. These are created in four delicate order grids of very coarse, coarse, medium and fine meshes which were used by Aboubacar et al. [6] as illustrated in Table 1 and Figure 2. All meshes are bias and the tiny elements (h_{min}) are placed next to the singularity.

(a) mesh1   (b) mesh2

(c) mesh3   (d) mesh4
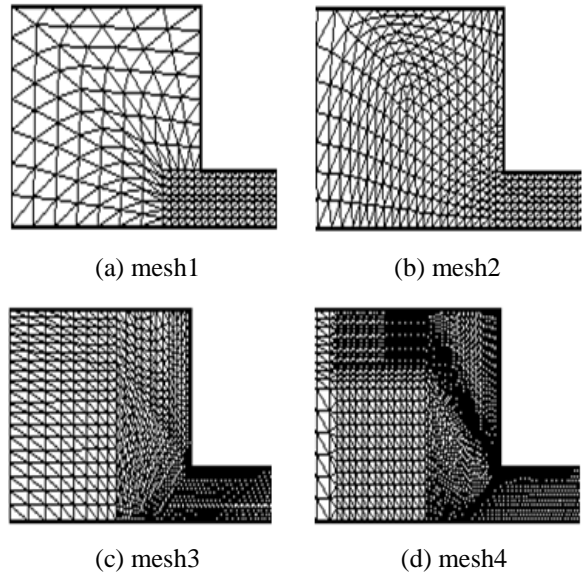
Figure 2: Sharp mesh pattern of 4:1 contraction flow.

5 Results

The results of sharp corner meshes are considered and the best mesh is selected to run for final solution in order to reduce duplicate outcome. After optimal mesh was taken, it was brought to run in both Newtonian and viscoelastic fluids under the condition of no slip and slip effect. The slip coefficients for each liquid are determined to adjust the flow pattern as displayed below.

5.1 *Newtonain fluid*

The peak values on top downstream wall with no slip of normal stress τ_{xx} and τ_{yy}, shear stress τ_{xy} and shear rate $\dot{\gamma}$ in Table 2 grow upon higher sensitivity of grid and we noticed that the peak of all values can classified in two groups of resemblance. The results of mesh1 and mesh2 are similar as well as mesh3 and mesh4 but the outcome of second group is prominent.

Table 2: The peak values of Newtonian fluid on top downstream wall with no slip

Mesh	τ_{xx}	τ_{xy}	τ_{yy}	$\dot{\gamma}$
mesh1	9.046	4.523	0.335	4.832
mesh2	9.014	4.507	0.330	4.753
mesh3	12.488	6.244	0.328	6.597
mesh4	15.998	8.000	0.325	8.660

In order to choose a suitable mesh to get the final solution, the dominant mesh will be selected, that is mesh3 or mesh4. For this case mesh3 is the best choice to prompt display even if mesh4 is fine net structure because the result of mesh3 can be run easier and faster to get converged solution than mesh4 whilst both grids give the little difference so the minor error can be negligible.
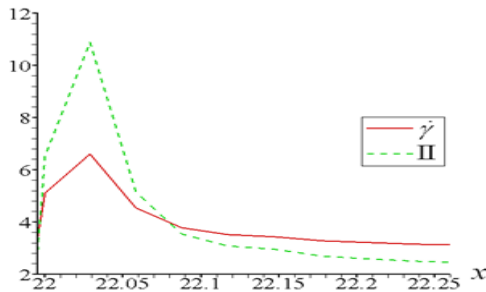
Figure 3: II and $\dot{\gamma}$ along top downstream wall with no slip of Newtonian fluid.

The similar behavior of second invariant (II) and shear rate $(\dot{\gamma})$ of Newtonian fluid for mesh3 are displayed in Figure 3. Both curves for II and $\dot{\gamma}$ look like a left-skewed distribution and the peaks are 10.881 and 6.597 for II and $\dot{\gamma}$, respectively. From the previous work, we found that all apexes go to

singularity in case of high *We* and these values are quite far from physical phenomena so it is the reason why slip condition is determined to reduce the zenith as see in Figure 4.

For choosing the optimum value of α and the critical II (II_{crit}), we used mesh3 to execute the slip effect for Newtonian fluid by running α from 0.1 to 1 as illustrated in Figure 4. First round of calculation to find minimum α of fixing $\text{II}_{crit} = 2.3$ for α at 0.3, 0.5, and 1 is observed that oscillations appear clearly but $\alpha = 0.1$ is ascertained properly the value of lowest peak $\dot{\gamma}$. This selection of minimum $\dot{\gamma}$ is supported by Figure 5 which displays a correlation between $\dot{\gamma}$ and α. Second round of computation to find the location of the critical II by setting $\alpha = 0.1$ and adjusting II from 0 to 10 is operated before relation of $\dot{\gamma}$ versus II_{crit} presents that the lowest II_{crit} points to 2.3 in Figure 6.
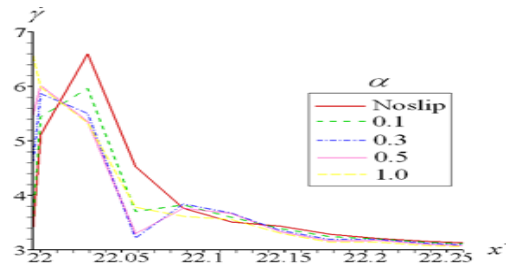
Figure 4: $\dot{\gamma}$ of various α along top downstream wall of Newtonian fluid at $\text{II} = 2.3$.
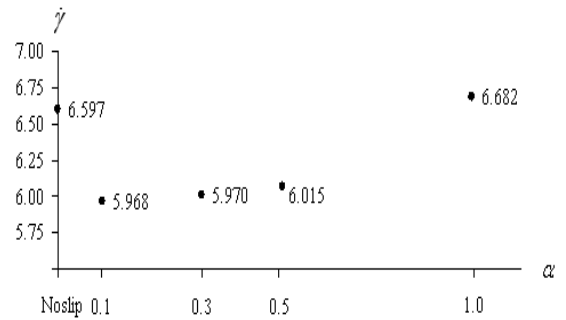
Figure 5: The peak of $\dot{\gamma}$ versus α on top downstream wall of Newtonian fluid at $\text{II} = 2.3$.
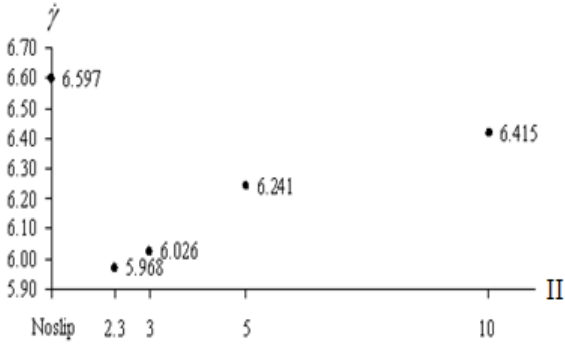
Figure 6: The peak of $\dot{\gamma}$ versus II_{crit} on top downstream wall of Newtonian fluid at $\alpha = 0.1$.

Figure 7 shows streamline (S) line contour for no slip in Figure 7(a) and slip effect at $\alpha = 0.1$, $\text{II} = 2.3$ in Figure 7(b). Graphs of both cases look similar but the vortex at the corner of no slip is bigger than that of its counterpart in the slip case.
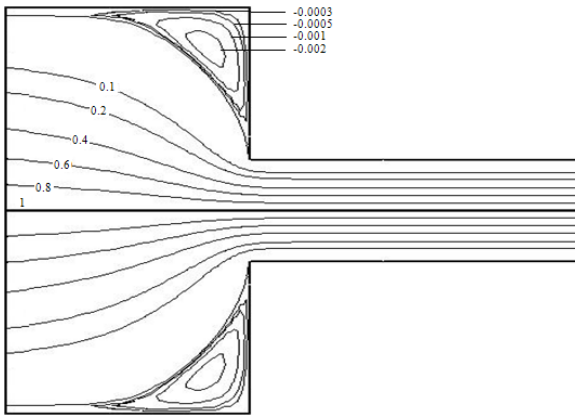
(a) no slip
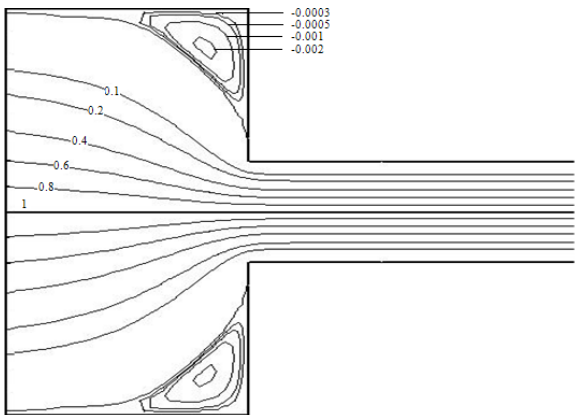
(b) slip at $\alpha = 0.1$ and $\text{II} = 2.3$

Figure 7: S line contour of Newtonian fluid.

5.2 *Oldroyd-B fluid*

For all meshes in Table 3, the viscoelastic fluids are considered for various We. The peak values on top downstream wall with no slip of normal stress $\dot{\gamma}$ grow upon high We and we observed that the peak of $\dot{\gamma}$ for all meshes have thrived with the same trend. The results of mesh1 and mesh2 are similar as well as mesh3 and mesh4 but the outcome of second group is prominent. Since the tendency of behavior for all We has the same direction, all sharp meshes are presented only $We = 1.0$ for all stresses $(\tau_{xx}, \tau_{xy}, \tau_{yy})$ with the same condition in Table 4. Mesh3 is chosen to run for the final solution for the same reasons stated earlier.

Table 3: The peak values of $\dot{\gamma}$ on top downstream wall with no slip of Oldroyd-B fluid

Mesh	0.25	0.5	0.75	1
mesh1	4.873	5.130	5.323	5.717
mesh2	4.929	5.061	5.153	5.510
mesh3	7.534	8.550	8.828	9.209
mesh4	8.833	9.380	9.504	10.234

Table 4: The peak values of τ_{xx}, τ_{xy} and τ_{yy} on the top downstream wall with no slip of Oldroyd-B fluid at $We = 1.0$

Mesh	τ_{xx}	τ_{xy}	τ_{yy}
mesh1	21.458	7.236	2.507
mesh2	22.512	8.047	3.018
mesh3	36.571	15.496	6.427
mesh4	37.670	15.068	8.772

To select critical II from Figure 8, we have considered the optimum α for $We = 0.25$ before calculation of high We via varying all α values between 0.1 and 1 so $\text{II} = 14$ is set first because the shear rate is high enough to switch some stick velocities to move freely. For choosing proper α by minimizing shear rate, the same procedure of Newtonian case is operated as seen in Figure 9 so the minimum shear rate is 7.530 at $\alpha = 0.1$ that is under the value of no slip condition while the other value of α has exceeded over the value of slip case. Other α

values are rejected except $\alpha = 0.1$ since the slip velocity decreases shear rate. By adjusting critical II, the range of II is started at 5 to 14 since the off range cannot be calculated for $\alpha = 0.1$ but the range II that is shown in Figure 10 and the least value shear rate for II = 6 is 7.175; therefore, the suitable coefficient slip is 0.1.

Similarly, the lowest shear rates of *We* = 0.5, 0.75, 1 for fitting critical II are shown in Table 5.

Figure 8: II on the top downstream wall without slip of Oldroyd-B fluid.
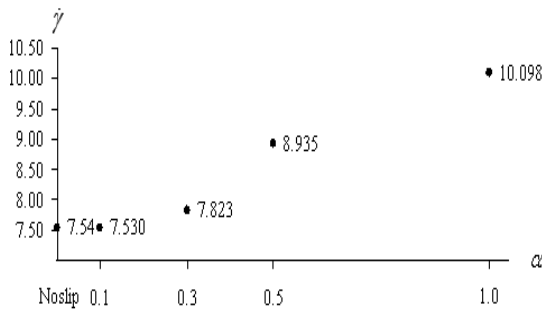
Figure 9: The peak of $\dot{\gamma}$ versus α on top downstream wall of Oldroyd-B fluid at *We* = 0.25 .
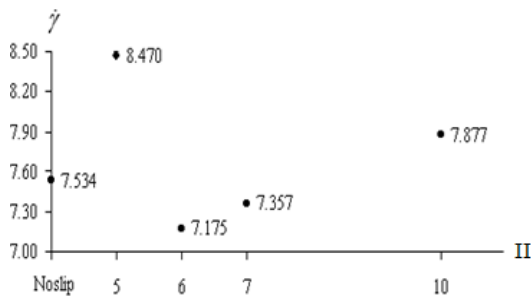
Figure 10: The peak of $\dot{\gamma}$ versus II_{crit} on top downstream wall of Oldroyd-B fluid at *We* = 0.25 .

To select critical II from Figure 8, we have considered the optimum α for *We* = 0.25 before calculation of high *We* via varying all α values between 0.1 and 1 so II = 14 is set first because the

shear rate is high enough to switch some stick velocities to move freely. For choosing proper α by minimizing shear rate, the same procedure of Newtonian case is operated as seen in Figure 9 so the minimum shear rate is 7.530 at $\alpha = 0.1$ that is under the value of no slip condition while the other value of α has exceeded over the value of slip case. Other α values are rejected except $\alpha = 0.1$ since the slip velocity decreases shear rate. By adjusting critical II, the range of II is started at 5 to 14 since the off range cannot be calculated for $\alpha = 0.1$ but the range II that is shown in Figure 10 and the least value shear rate for II = 6 is 7.175; therefore, the suitable coefficient slip is 0.1.

Similarly, the lowest shear rates of *We* = 0.5, 0.75, 1 for fitting critical II are shown in Table 5.

Table 5: The lowest shear rate for proper α and suitable II of Oldroyd-B fluid

We	0	0.25	0.5	0.75	1
α	0.1	0.1	0.1	0.1	0.1
II_{crit}	2.3	6	4	3.5	3.3
$\dot{\gamma}$	5.968	7.175	7.554	8.611	8.801

Summarizing the highest τ_{xx} and the maximum shear rate values of the optimum slip velocity in Table6 are less than the maximum values of no slip condition. The maximum value of τ_{xx} is reduced from 19.943 to 13.494 and the peak of $\dot{\gamma}$ is reduced from 7.534 to 7.1745 at *We* = 0.25 . Similar to the trend of the slip influence for *We* at 0.5, 0.75 and 1, the maximum of $\dot{\gamma}$ and τ_{xx} without slip falls below that for the case with slip. Highly reducing the stress value is clearly investigated, refer to Table 5.

Table 6: The peak value of $\dot{\gamma}$ and τ_{xx} on the top downstream wall

We	$\dot{\gamma}$		τ_{xx}	
	no Slip	Slip	no Slip	Slip
0.25	7.534	7.175	19.943	13.494
0.5	8.550	7.554	29.455	20.586
0.75	8.828	8.611	34.042	30.975
1	9.253	8.721	36.571	34.557

(a) $We = 0.25$

(b) $We = 1.0$
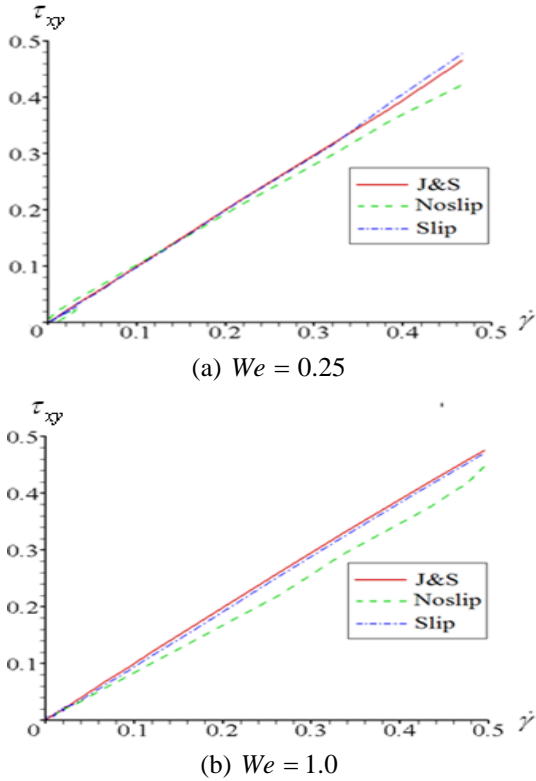
Figure 11: The comparison of τ_{xy} versus $\dot{\gamma}$ with J&S on top downstream wall of Oldroyd-B fluid.

Figure 11 shows the comparison of two restrictions under condition of no-slip and slip along bottom downstream wall with J&S (Johnson-Segalman) theory from equation (4) by relating τ_{xy} and $\dot{\gamma}$ at $We = 0.25$ and $We = 1.0$. This plot is indicative of the fact that the shear stress of both cases agree in trend along the resistance but slip limitation is closer to J&S though the value of prediction is slightly undershoot.

If we compare the streamline of Figure 12(a) for no slip and Figure 12(b) for slip, the serious vortex is still noticed easily for no slip case so this observation can get along well with Oldroyd-B behaviour.

(a) no slip

(b) slip at $\alpha = 0.1$ and $\mathrm{II} = 3.3$
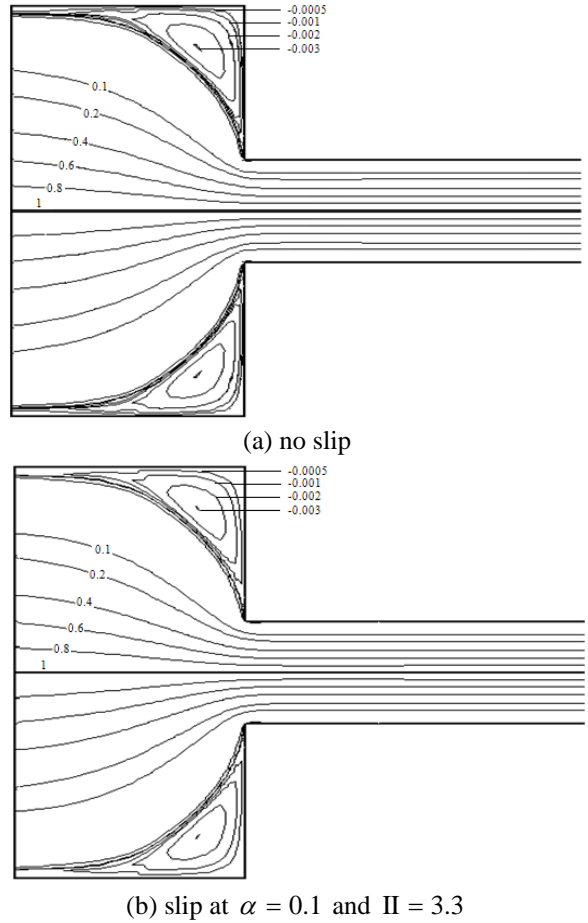
Figure 12: S line contour of Oldroyd-B at $We = 1.0$

As stated above (the reason for using $We = 1.0$ for final solution), Figure 13 depicts the line contour of slip condition for $\alpha = 0.1$ in line with the following explanation: Figure 13(a) shows the maximum value of velocity u at symmetry line, Figure 13(b) displays the maximum value of velocity v near the location of sharp corner contraction position, Figure13(c) represents line contour of maximum pressure inlet boundary, the maximum τ_{xx}, τ_{xy} and τ_{yy} as can be seen in Figures 13(d)-13(f) are 34.042, 14.505, and 7.116, respectively.

(a) u

(b) v

(c) P

(d) τ_{xx}

(e) τ_{xy}

(f) τ_{yy}
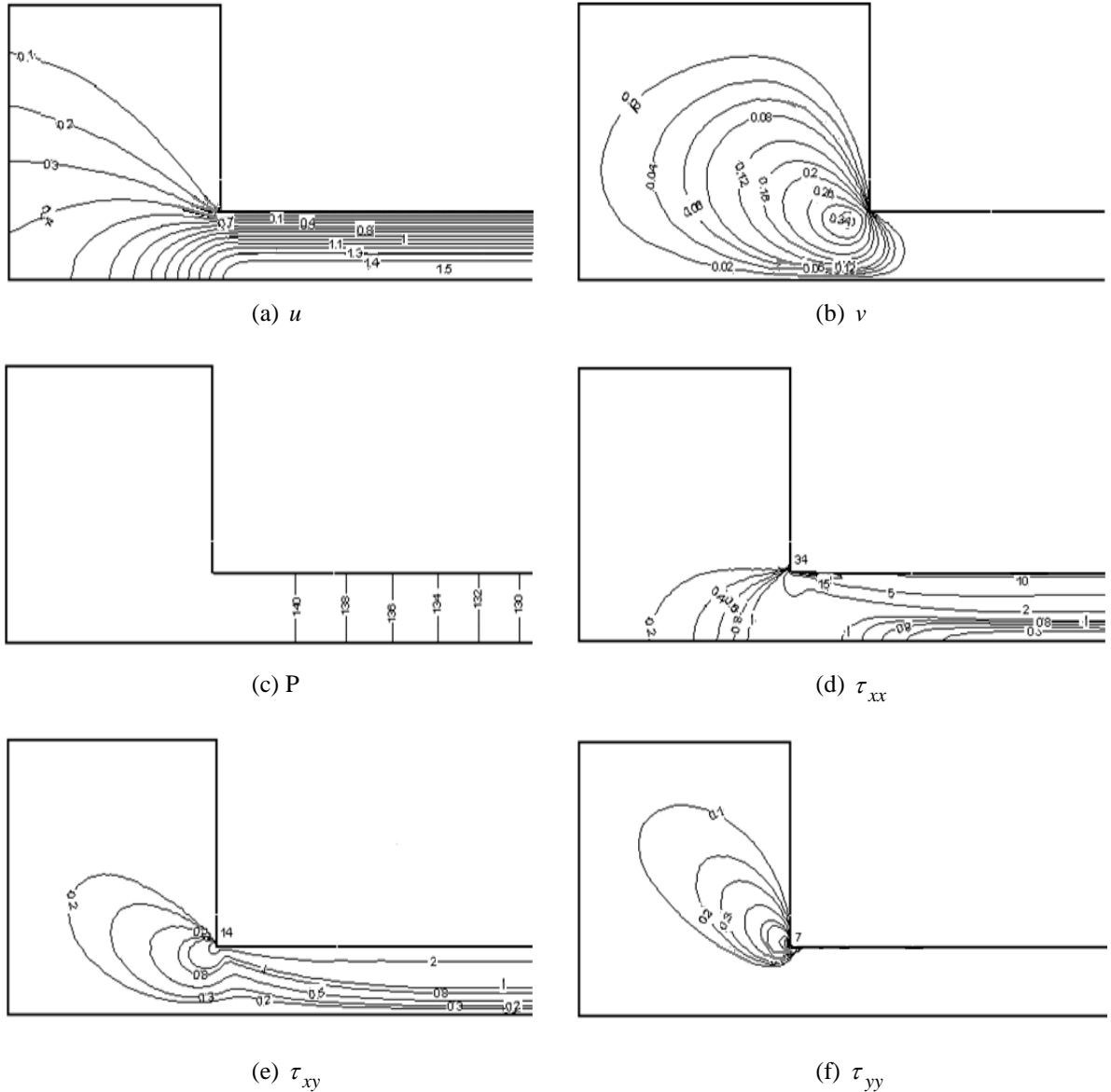
Figure 13: Line contour with slip along top downstream wall of Oldroyd-B fluid at $\alpha = 0.1$, II $= 3.3$ and $We = 1.0$.

6   Conclusions

For the results of slip effect in 4:1 contraction problem, we found that the optimum slip coefficient of all We is 0.1 if we adjust the appropriate critical II. The appropriate values of the slip coefficient and the second invariant cause the peak of shear rate lower than no-slip case. Hence it can be concluded that the slip well reduces the stress along the wall. In the same direction, when the small We is input, the less effect is appeared and this is reversed with high Weissenberg numbers.

and Computer Science, Faculty of Science, Chulalongkorn University to sustain the advanced computer machinery.

References

[1] Boger D.V. and Ramamurthy A. V., 1972. Flow of Viscoelastic Fluids though an Abrupt Contraction, *Rheol. Acta*., 11: 61-69.

[2] Boger D.V. and Denn M. M., 1980. Capillary and Slit Methods of Normal Stress Measurements, *Non-Newtonian Fluid Mech*., 6: 163-185.

[3] Walters K. and Rawlinson D. M., 1982. On some Contraction Flows for Boger Fluid, *Rheol. Acta*., 21: 547-552.

[4] Boger D.V., 1987. Viscoelastic Flows through Contractions, *Ann. Rev. Fluid Mech*., 19: 157–182.

[5] Phillips T.N. and Williams A.J., 1999. Viscoelastic Flow through a Planar Contraction Using a Semi-Lagrangian Finite Volume Method, *J. Non-Newtonian Fluid Mech*., 87: 215–246.

[6] Phillips T.N. and Williams A.J., 2002. Comparison of Creeping and Inertial Flow of an Oldroyd-B Fluid through Planar and Axisymmetric Contractions, *J. Non-Newtonian Fluid Mech*., 108: 25–47.

[7] Aboubacar M. and Webster M.F., 2001. A Cell-Vertex Finite Volume/Element Method on Triangles for Abrupt Contraction Viscoelastic Flows, *J. Non-Newtonian Fluid Mech*., 98: 83–106.

[8] Aboubacar M., Matallah H. and Webster M.F., 2002. Highly Elastic Solutions for Oldroyd-B and Phan-Thien/Tanner Fluids with a Finite Volume/Element Method: Planar Contraction Flows, *J. Non-Newtonian Fluid Mech*., 103: 65–103.

[9] Alves M.A., Torres D., Goncalves M.P., Oliverira P.J. and Pinho F.T., 2004. On the Effect of Contraction Ratio in Viscoelastic Flow through Abrupt Contractions, *J. Non-Newtonian Fluid Mech*., 122: 117–130.

[10] Ngamaramvaranggul V. and Webster M. F., 2001. Viscoelastic Simulation of Stick-slip and Die-swell Flows, *Int. J. Num. Meth. Fluids*., 36: 539-595.

[11] Ngamaramvaranggul V. and Webster M. F., 2002. Simulation of Pressure-Tooling Wire-Coating Flows with Phan-Thien/Tanner Models, *Int. J. Num. Meth. Fluids*, 38: 677-710.

[12] Belblidia F., Matallah H. , Puangkird B. and Webster M.F., 2007. Alternative Subcell Discretisations for Viscoelastic Flow : Stress Interpolation. *J. Non-Newtonian Fluid Mech*., 146: 59–78.

[13] Puangkird B., Belblidia F. and Webster M.F., 2009. Numerical Simulation of Viscoelastic Fluids in Cross-Slot Devices. *J. Non-Newtonian Fluid Mech*., 162: 1–20.

[14] Silliman W. J. and Scriven L. E., 1980. Separating Flow Near a Static Contact Line: Slip at a Wall and Shape of a Free Surface, *J. Comp. Phys*., 34: 287-313.

[15] Ramamurthy A. V., 1986. Wall Slip in Viscous Fluids and Influence of Materials of Construction, *J. Rheol*., 30: 337-357.

[16] Jiang T. Q., Young A. C. and Metzner A. B., 1986. The Rheological Characterization of HPG Gels: Measurement of Slip Velocity in Capillary Tubes, *Rheol. Acta*, 25(4): 397-404.

[17] Phan-Thien N., 1988. Influence of Wall Slip on Extrudate Swell: a Boundary Element Investigation, *J. Non-Newtonian Fluid Mech*., 26: 327-340.

[18] Ngamaramvaranggul V. and Webster M. F., 2000. Simulation of Coating Flows with Slip Effects, *Int. J. Num. Meth. Fluids*., 33: 961-992.

[19] Johnson M.W. and Segalman D., 1977. A Model for Viscoelastic Fluid Behavior Which Allows Non-Affine Deformation, *J. Non-Newtonian Fluid Mech*., 2: 255-270.